Materials Transactions, Vol. 44, No. 9 (2003) pp. 1895 to 1898

RAPID PUBLICATION

Structure and Properties of Melt-Spun Mg–Pd Binary Alloys

Shin-ichi Yamaura*, Hisamichi Kimura and Akihisa Inoue

Institute for Materials Research, Tohoku University, Sendai 980-8577, Japan

Amorphous alloys in the Mg–Pd binary system were formed in a composition range of 10 to 35 at%Pd by melt-spinning technique. The crystallization temperature and tensile strength of the amorphous $Mg_{100-x}Pd_x$ ($x = 10$, 20 and 30 at%) alloys are in the range from 417 to 535 K and 440 to 650 MPa, respectively. There is a tendency for the crystallization temperature and the tensile strength to increase with increasing Pd content. Vickers hardness also increased with increasing Pd content. Their compositional dependence is attributed to an increase in the number of Mg–Pd atomic pairs with large negative mixing enthalpy. Crystallized structure of the Mg–Pd amorphous alloys was also examined in correlation with equilibrium phases.

(Received June 10, 2003; Accepted July 29, 2003)

Keywords: *amorphous, melt-spinning, magnesium–palladium (Mg–Pd) alloy*

1. Introduction

Recently, Mg-based alloys have attracted increasing interest because of their useful engineering properties such as high strength with light weight[1)] and high hydrogen-storage capacity.[2)] It is well known that the structural modification to an amorphous phase significantly increases various properties as compared with crystalline alloys.[3)] An amorphous phase has been formed in a number of Mg-based alloy systems such as Mg–Cu[4)] and Mg–Ln-TM (Ln = lanthanide metal).[5)] Particularly, the Mg–Ln-TM alloys are important because they have a large supercooled liquid region before crystallization and high glass-forming ability.[6)] It has subsequently been reported that the plateau region in electrochemically measured P-C isotherm and high electrochemical discharge capacity are obtained in Mg–Ni[7,8)] and Mg–Ni–Pd[9)] amorphous alloys. In addition to Mg–Ni amorphous alloys, Mg–Pd-based amorphous alloys are also expected as a base alloy system to develop useful functional materials with high hydrogen absorption ability. However, there have been no data on the formation of an amorphous alloy in Mg–Pd binary system. Furthermore, little has been reported about the formation of Mg-based amorphous alloy with high Mg content above 85 at% except the Mg–Ni binary system. Therefore, this paper intends to present the composition range in which an amorphous phase is formed in Mg–Pd binary system by melt-spinning and intends to investigate the reason for the formation of the amorphous phase even at the Mg-rich compositions. The thermal stability and mechanical properties of the Mg–Pd amorphous alloys were also studied in this work.

2. Experimental Procedure

Mg–Pd binary alloy ingots were prepared by high-frequency induction melting the mixtures of pure Mg and Pd metals in an Ar atmosphere. Ribbons of about 20 μm in thickness and about 1 mm in width were produced by a single-roller melt-spinning technique in an Ar atmosphere. The circumferential velocity of the wheel (v_c) was controlled as 40 m/s. The structure of the melt-spun ribbons was examined by X-ray diffractometry (XRD; Cu-Kα, 35 kV, 15 mA) and by Transmission Electron Microscopy (TEM). Crystallization temperature (T_x) was examined by differential scanning calorimetry (DSC) at a heating rate of 0.67 K/s. Tensile fracture strength was measured at a strain rate of $8 \times 10^{-4}\ s^{-1}$ with an Instron-type testing machine. Hardness was also measured by a Vickers microhardness tester with a load of 10–25 g.

3. Results and Discussion

Figure 1 shows XRD patterns of the melt-spun $Mg_{100-x}Pd_x$ ($x = 2$, 4, 6, 8, 10, 20, 30 and 40 at%) alloys. Distinct crystalline peaks of Mg phase are seen in the XRD patterns of the $Mg_{100-x}Pd_x$ ($x = 2$, 4, 6 and 8 at%) alloys. Intensity of the sharp peaks decreases with increasing Pd content from 2 to 8 at% and no crystalline peak is observed at 10 at% Pd. Only broad diffraction peaks are seen for the $Mg_{100-x}Pd_x$ ($x = 10$, 20 and 30 at%) alloys, indicating the formation of an amorphous phase. Sharp crystalline peaks are also seen in the XRD pattern of the $Mg_{60}Pd_{40}$ alloy. The sharp peaks of the 40 at%Pd alloy may come from MgPd phase according to the previous reports,[10,11)] though there is no data in the ICDD cards on the XRD patterns of Mg_4Pd, Mg_3Pd and MgPd alloys.

Figure 2 summarizes the composition range in which amorphous Mg–Pd alloys are formed by melt-spinning, together with the Mg–Pd binary phase diagram.[12)] The amorphous phase is formed in a composition range of 10 to 35 at%Pd. According to the Mg–Pd phase diagram, a eutectic point is located at 7.8 at%Pd. Therefore, it is understandable that the minimum Pd content at which the Mg–Pd amorphous phase can be formed lies near the eutectic composition. The upper limitation of Pd content for the formation of the amorphous phase may be due to the increase in melting point.

Figure 3 shows bright-field TEM images of the melt-spun (a) $Mg_{92}Pd_8$ and (b) $Mg_{90}Pd_{10}$ alloys. No crystalline phase is seen in the melt-spun $Mg_{90}Pd_{10}$ alloy while fine crystalline particles are recognized in the $Mg_{92}Pd_8$ alloy. A halo-type diffraction ring pattern for the $Mg_{90}Pd_{10}$ alloy was also obtained while reflection spots were observed for the

*Corresponding author, E-mail: yamaura@imr.tohoku.ac.jp

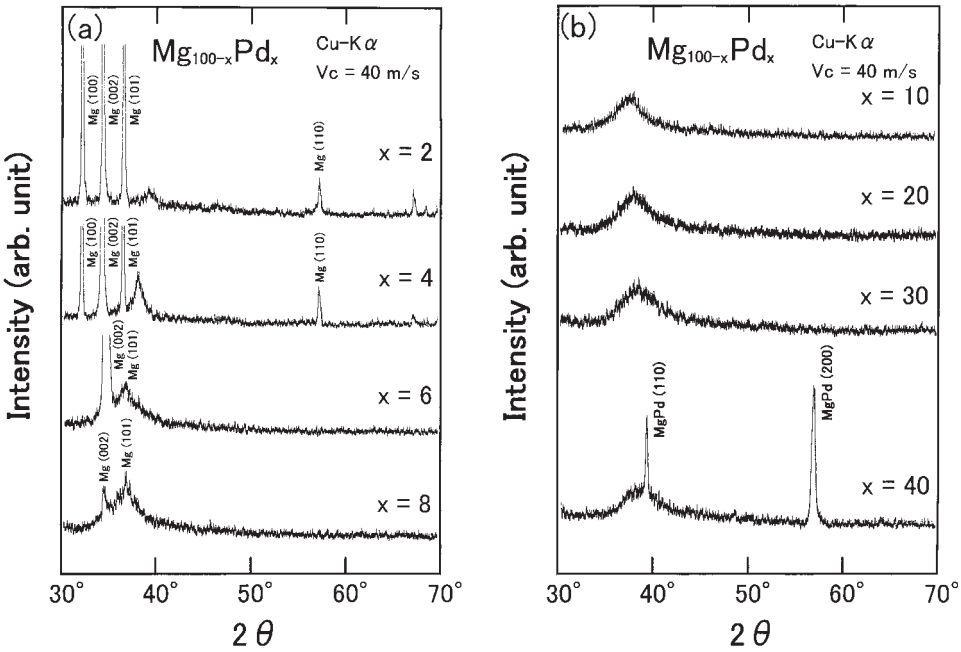

Fig. 1 XRD patterns of melt-spun $Mg_{100-x}Pd_x$ ($x = 2$, 4, 6, 8, 10, 20, 30 and 40 at%) alloys.

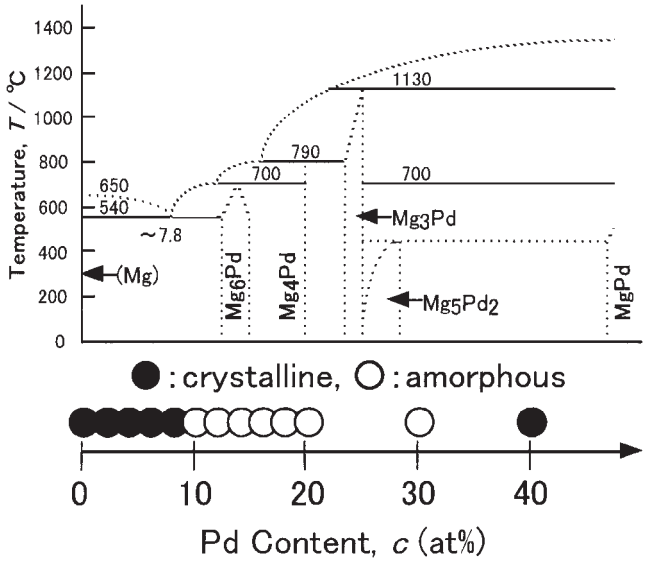

Fig. 2 Composition dependence of structure in melt-spun Mg–Pd alloys, ○: amorphous; ●: crystalline.

$Mg_{92}Pd_8$ alloy.

Figure 4 shows DSC curves of the amorphous $Mg_{100-x}Pd_x$ ($x = 10$, 20 and 30 at%) alloys. No supercooled liquid region is observed before crystallization. The crystallization temperature, T_x increases with increasing Pd content, indicating that the thermal stability of the amorphous phase is improved with Pd content. It is also seen that the number of crystallization peaks decreases with increasing Pd content. The crystallization process changes into a more simple mode for the higher Pd content alloys.

Crystalline phases appeared in the $Mg_{100-x}Pd_x$ ($x = 10$, 20 and 30 at%) amorphous alloys after heat treatment were identified by XRD observation. The samples annealed for 1 h at the temperature just below the first crystallization peak in evacuated quartz tubes were used to know the first-stage crystallization behavior of the $Mg_{90}Pd_{10}$ and the $Mg_{80}Pd_{20}$ amorphous alloys. Heat treatment was also performed by using the DSC equipment to know the crystallization behavior for second and third exothermic peaks. The samples were cooled rapidly soon after recognizing the appearance of the crystallization peak in the DSC curve at which we would like to identify the crystallization process. Figure 5 shows the XRD patterns of the $Mg_{90}Pd_{10}$ amorphous alloy after heat treatments. The first-stage crystallization was examined by heating the sample at 400 K for 1 h. It is seen that the first exothermic peak is due to the precipitation of Mg phase and the second peak comes from the precipitation of Mg_6Pd phase from the remaining amorphous phase. The third peak appears to correspond to the transition to Mg + Mg_6Pd + unknown phases.

Figure 6 shows the XRD patterns of the $Mg_{80}Pd_{20}$ amorphous alloy subjected to the heat treatments corresponding to the two exothermic peaks. The first-stage crystallization was examined by heating the sample at 473 K for 1 h. The crystallization occurs through Am → Am + unknown phase → unknown + Mg_6Pd and Mg_5Pd_2. Although the unknown phase at the first crystallization peak is predicted as Mg_4Pd or Mg_3Pd phase on the basis of the Mg–Pd equilibrium phase diagram, no X-ray diffraction data of their phases are observed.

Figure 7 shows the XRD pattern of the $Mg_{70}Pd_{30}$ amorphous alloy heated up to 570 K in the DSC equipment. Both Mg_5Pd_2 and unknown phases are observed. The unknown phase cannot be identified as Mg_3Pd or MgPd which is predicted from the Mg–Pd equilibrium phase diagram.

Table 1 summarizes crystallization temperature, T_x, tensile strength, σ_f and Vickers hardness, Hv of melt-spun amorphous $Mg_{100-x}Pd_x$ ($x = 10$, 20 and 30 at%) alloys. There is a tendency for T_x, σ_f and Hv to increase with increasing Pd

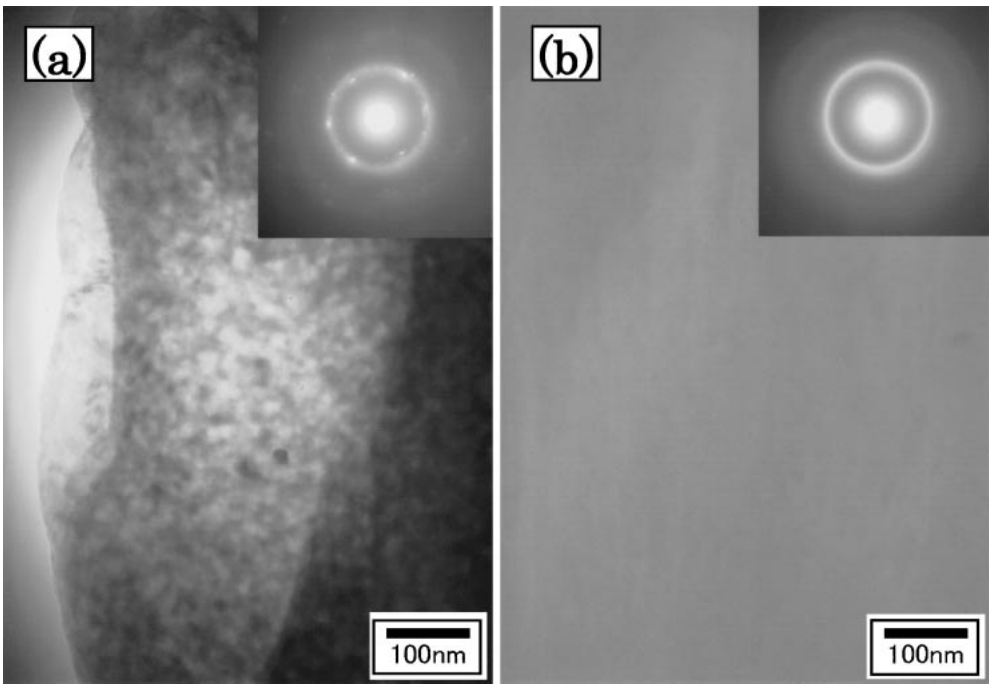

Fig. 3 TEM bright-field images and diffraction rings of melt-spun (a) $Mg_{92}Pd_8$ and (b) $Mg_{90}Pd_{10}$ alloys.

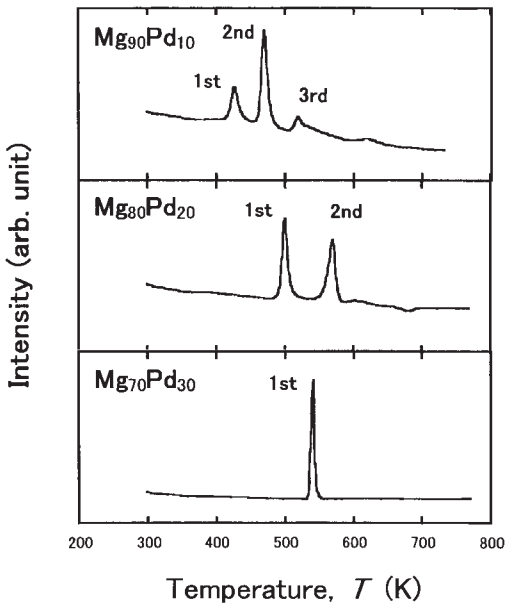

Fig. 4 DSC curves of melt-spun $Mg_{100-x}Pd_x$ ($x = 10$, 20 and 30 at%) alloys.

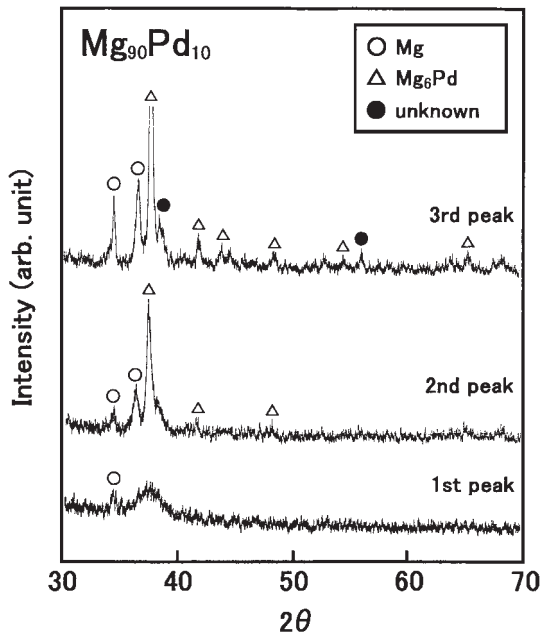

Fig. 5 Identification of precipitated crystalline phases appeared at the three distinct crystallization exothermic peaks.

content. The $Mg_{60}Pd_{40}$ crystalline alloys are too brittle to measure the tensile fracture strength.

Inoue *et al.* reported that the composition range of Mg–Ni binary amorphous alloys was limited to $8 < \mathrm{Ni} < 25$ at%Ni.[6] It is known that the feature of the Mg–Pd equilibrium phase diagram is similar to that of the Mg–Ni phase diagram because Pd belongs to the same group number as that of Ni. In this work, it was shown that the composition range of the Mg–Pd binary amorphous alloys was limited to $10 < \mathrm{Pd} < 35$ at%Pd. Thus, the composition range of the Mg–Pd amorphous alloys is slightly wider than that for the Mg–Ni amorphous alloys. The mixing enthalpies of Mg–Pd and Mg–Ni pairs are -40 kJ/(mole of atoms) and -4 kJ/(mole of atoms), respectively.[13] These data suggest that the amorphous phase is produced more easily in the Mg–Pd system having the larger negative mixing enthalpy than in the Mg–Ni system.

4. Conclusions

We examined the structure, thermal stability and mechanical properties of the melt-spun Mg–Pd binary alloys. The results obtained are summarized as follows.

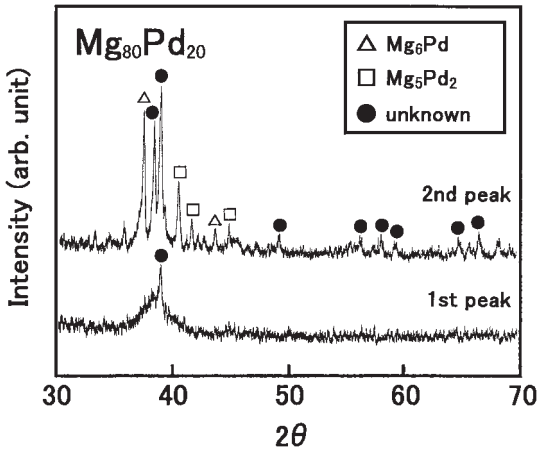

Fig. 6 Identification of precipitated crystallization phases appeared at the two distinct crystallization exothermic peaks.

Table 1 Summary of crystallization temperature, T_x, tensile strength, σ_f and Vickers hardness, Hv of melt-spun amorphous $Mg_{100-x}Pd_x$ ($x = 10$, 20 and 30 at%) binary alloys.

Pd content (at%)	T_x (K)	σ_f (MPa)	Hv
10	417	440	200
20	492	630	315
30	535	650	354

(1) Amorphous alloys in the Mg–Pd system were formed in a composition range of 10 to 35 at%Pd.
(2) Crystallization of the amorphous phase takes place through three-stage reactions of Am → Am + Mg → Am + Mg + Mg_6Pd → Mg + Mg_6Pd + unknown for the $Mg_{90}Pd_{10}$ alloy, two-stage reactions of Am → Am + unknown → Mg_5Pd_2 + Mg_6Pd + unknown for the $Mg_{80}Pd_{20}$ alloy and single-stage reaction of Am → Mg_5Pd_2 + unknown for the $Mg_{70}Pd_{30}$ alloy.
(3) The T_x, σ_f and Hv of the amorphous $Mg_{100-x}Pd_x$ ($x = 10$, 20 and 30 at%) alloys are in the range from 417 to 535 K, 440 to 650 MPa and 200 to 354, respectively. There is a tendency for T_x, σ_f and Hv to increase with increasing Pd content. The tendency is due to an increase in the number of Mg–Pd atomic pairs with large negative mixing enthalpy.

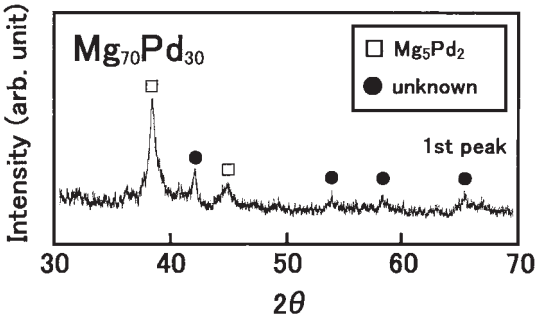

Fig. 7 Identification of precipitated crystallization phases appeared at a distinct crystallization exothermic peak.

REFERENCES

1) A. Inoue, K. Ohtera, K. Kita and T. Masumoto: Jpn. J. Appl. Phys. **27** (1988) L2248-L2251.
2) J. J. Reilly and R. H. Wishall: J. Inorg. Chem. **7** (1968) 2254–2256.
3) A. Inoue: Mater. Trans., JIM **36** (1995) 866–875.
4) A. Suganuma, T. Kato, H. Horikiri, Y. Kawamura, A. Inoue and T. Masumoto: Cryst. Res. Technol. **1** (1993) 112–117.
5) M. Matsuura, T. Fukunaga and U. Mizutani: Cryst. Res. Technol. **1** (1993) 464–468.
6) A. Inoue, M. Kohinata, A. P. Tsai and T. Masumoto: Mater. Trans., JIM **30** (1989) 378–381.
7) S. Orimo, A. Zuettel, K. Ikeda, S. Saruki, T. Fukunaga, H. Fujii and L. Schlapbach: J. Alloy. Compd. **293–295** (1999) 437–442.
8) S. Nohara, N. Fujita, S. G. Zhang, H. Inoue and C. Iwakura: J. Alloy. Compd. **267** (1998) 76–78.
9) S. Yamaura, H. Y. Kim, H. M. Kimura, A. Inoue and Y. Arata: J. Alloy. Comp. **347** (2002) 239–243.
10) in *Pearson's Handbook of Crystallographic Data for Intermetallic Phases -2nd Edition-*, Eds., P. Villars and L. D. Calvert, (ASM International, 1991).
11) R. Ferro: J. Less-Common Met. **1** (1959) 424–438.
12) A. A. Nayeb-Hashemi and J. B. Clark: Bull. Alloy Phase Diagrams **6** (1985) 164–167.
13) in *COHESION IN METALS -TRANSITION METAL ALLOYS-*, Eds., F. R. de Boer *et al.*, (Elsevier Science Publishers B.V., 1988).